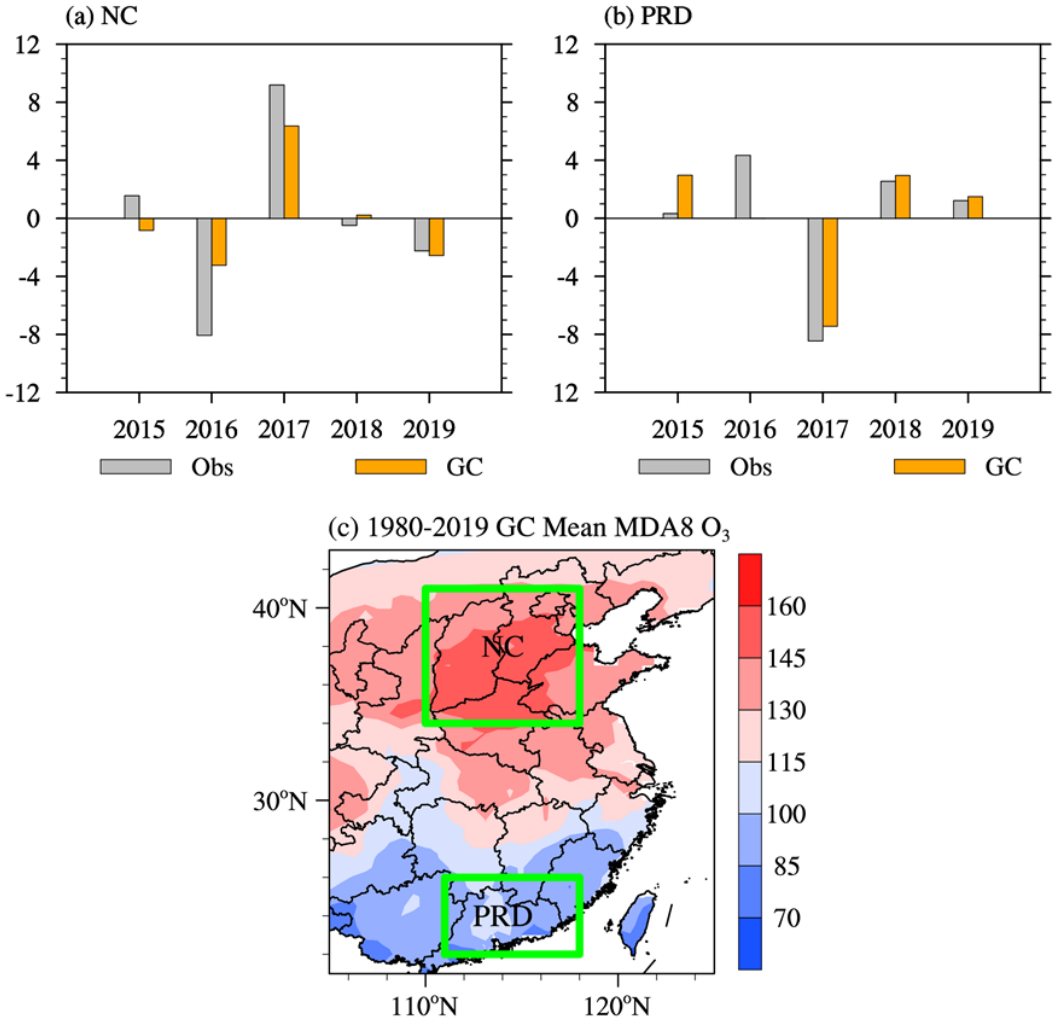

Figure S1. Histogram of JJA mean observed (gray) and simulated (orange) MDA8 O_3 after detrending in NC (a) and PRD (b) from 2015 to 2019. (c) Spatial distribution of GEOS-Chem simulated MDA8 O_3 (unit: μg m^{-3}) in summer from 1980 to 2019. The simulated O_3 concentrations were produced by GEOS-Chem with fixed emissions but changing meteorological conditions from 1980 to 2019. The green boxes in panels (c) indicate the locations of NC and PRD.

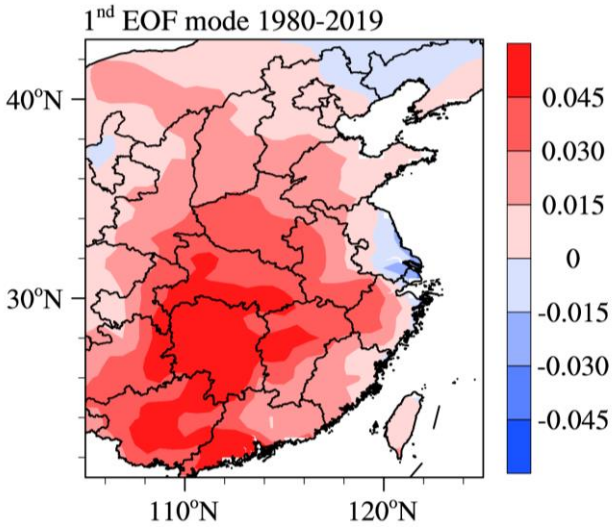

Figure S2. The first EOF pattern of simulated MDA8 O_3 in summer from 1980 to 2019. The simulated O_3 concentrations were produced by GEOS-Chem with fixed emissions but changing meteorological conditions.

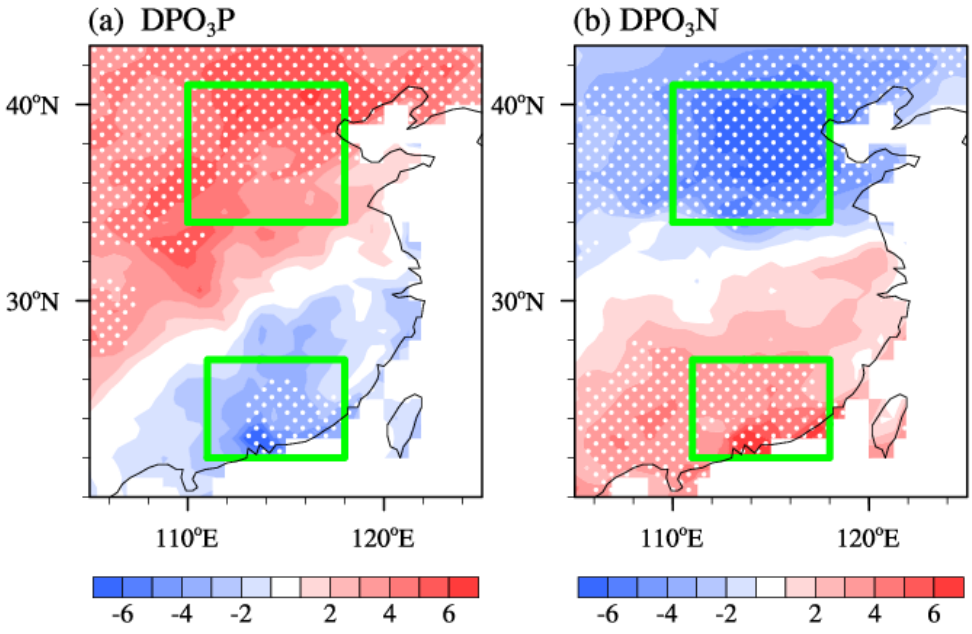

Figure S3. Composites of the simulated MDA8 O_3 (unit: μg m^{-3}) after detrending for DPO_3 in summer from 1980 to 2019. Panel (a) is composited when the time coefficient of DPO_3 is greater than one standard deviation (DPO_3P), while panels (b) is composited when the time coefficient is less than −1 × a standard deviation (DPO_3N). The green box in panels (a) and (b) are the NC and PRD areas.

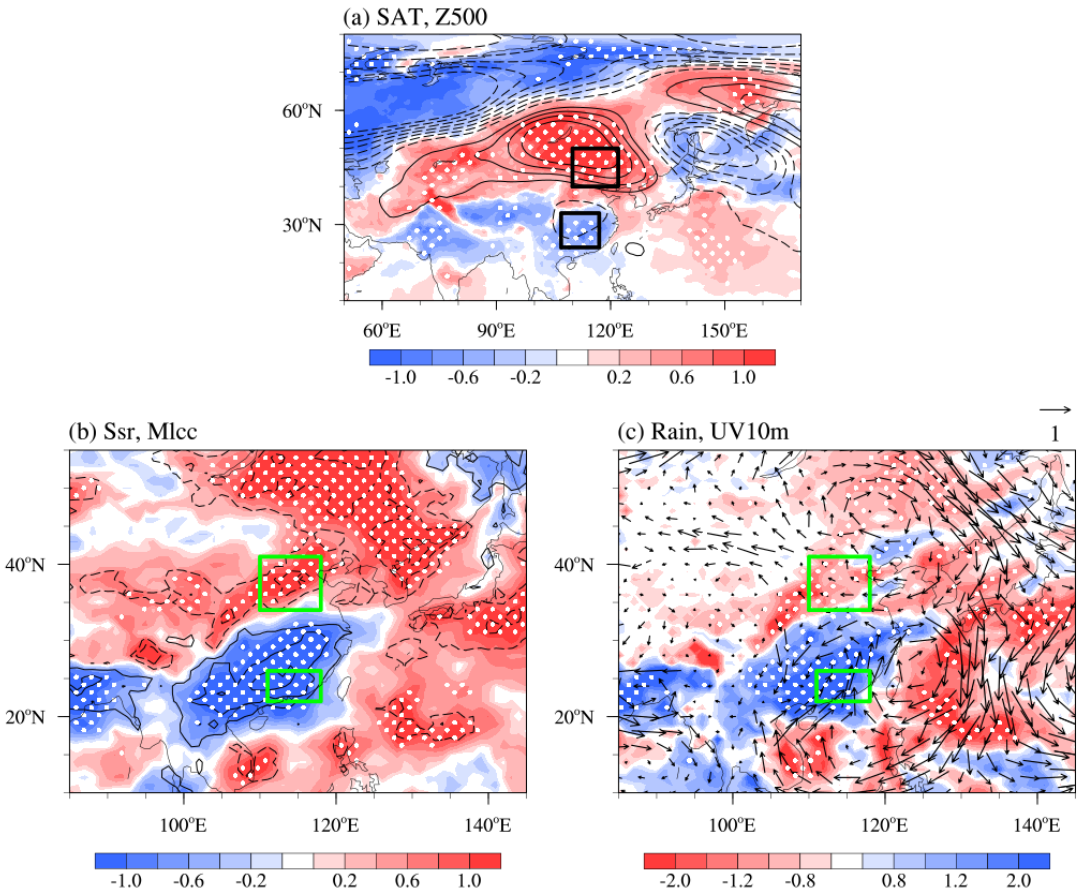

Figure S4. Composites of summer atmospheric circulations associated with the SI_{FJL} ($SI_{FJL}P$ minus $SI_{FJL}N$) from 1980 to 2019: (a) surface air temperature (unit: K, shading) and geopotential height at 500 hPa (unit: gpm, contours), (b) downward solar radiation at the surface (unit: 10^6 J m^{-2}, shading) and the sum of low and medium cloud cover (unit: 1, contours), and (c) precipitation (unit: mm, shading) and surface wind (unit: m s^{-1}, arrows). The white dots indicate that the differences with shading was above the 90% confidence level. The green boxes in panels (b) and (c) are the NC and PRD regions. The black boxes in panel (a) mean the centers of the AAC_{NC} and AC_{PRD}, respectively.

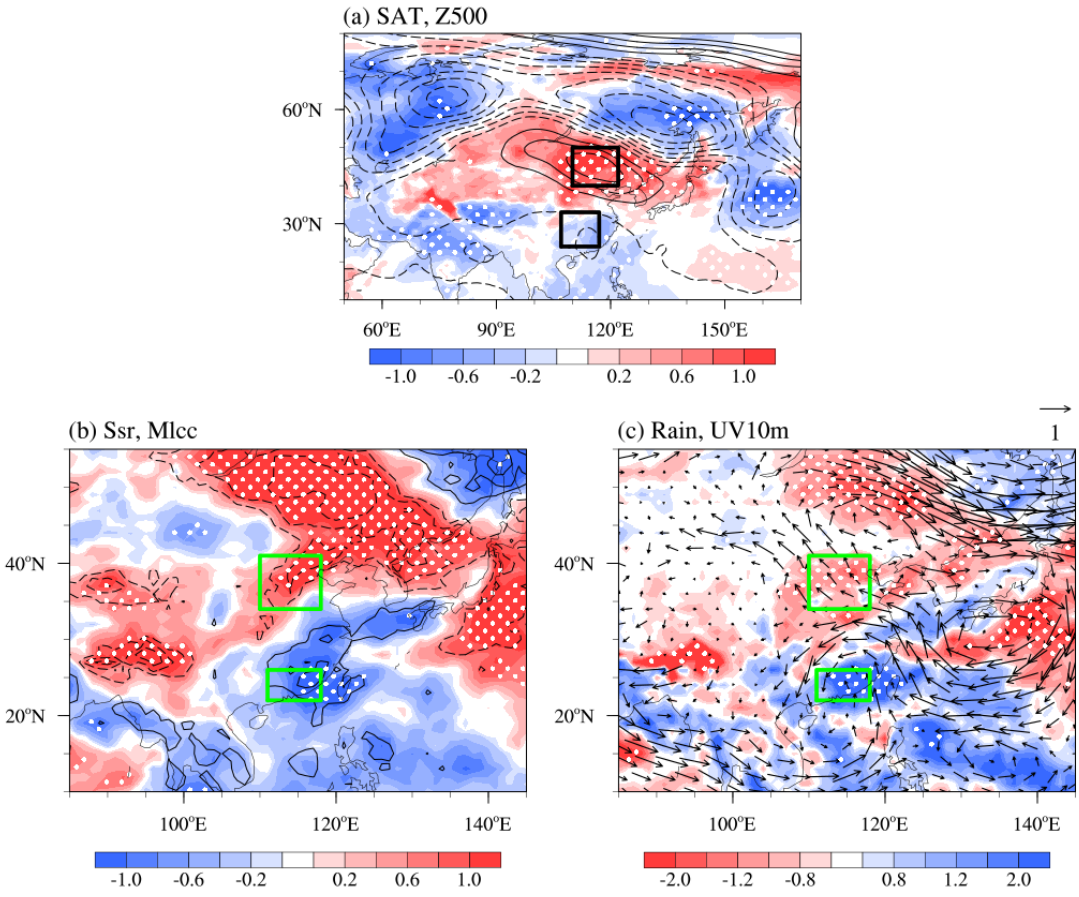

41

42 **Figure S5.** Composites of summer atmospheric circulations associated with the SIOD (SIODP minus SIODN) from 1980 to
43 2019: (a) surface air temperature (unit: K, shading) and geopotential height at 500 hPa (unit: gpm, contours), (b) downward
44 solar radiation at the surface (unit: 10^6 J m^{-2}, shading) and the sum of low and medium cloud cover (unit: 1, contours), and (c)
45 precipitation (unit: mm, shading) and surface wind (unit: m s^{-1}, arrows). The white dots indicate that the differences with
46 shading was above the 90% confidence level. The green boxes in panels (b) and (c) are the NC and PRD regions. The black
47 boxes in panel (a) mean the centers of the AAC_{NC} and AC_{PRD}, respectively.

48

49

50

51

52

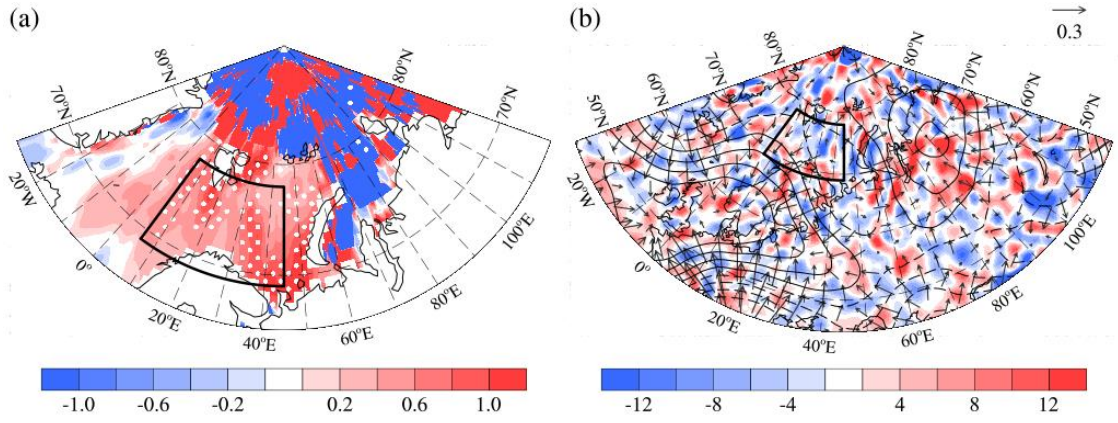

Figure S6. Composites of summer (a) Arctic SST (unit: K) on the time series of sign reversed SI_{FJL} index ($SI_{FJL}N$ minus $SI_{FJL}P$). The black box is used to calculate the Arctic SST index associated with SI_{FJL} in panels (a). The white dots indicate that the differences with shading was above the 90% confidence level. (b) Composites of JJA Rossby wave source (unit: 10^{-11} s^{-2}, shading), velocity potential (unit: 10^5 m^2 s^{-1}, contour) and divergent wind (unit: m s^{-1}, vector) at 500 hPa on the time series of the Arctic SST index associated with SI_{FJL}.

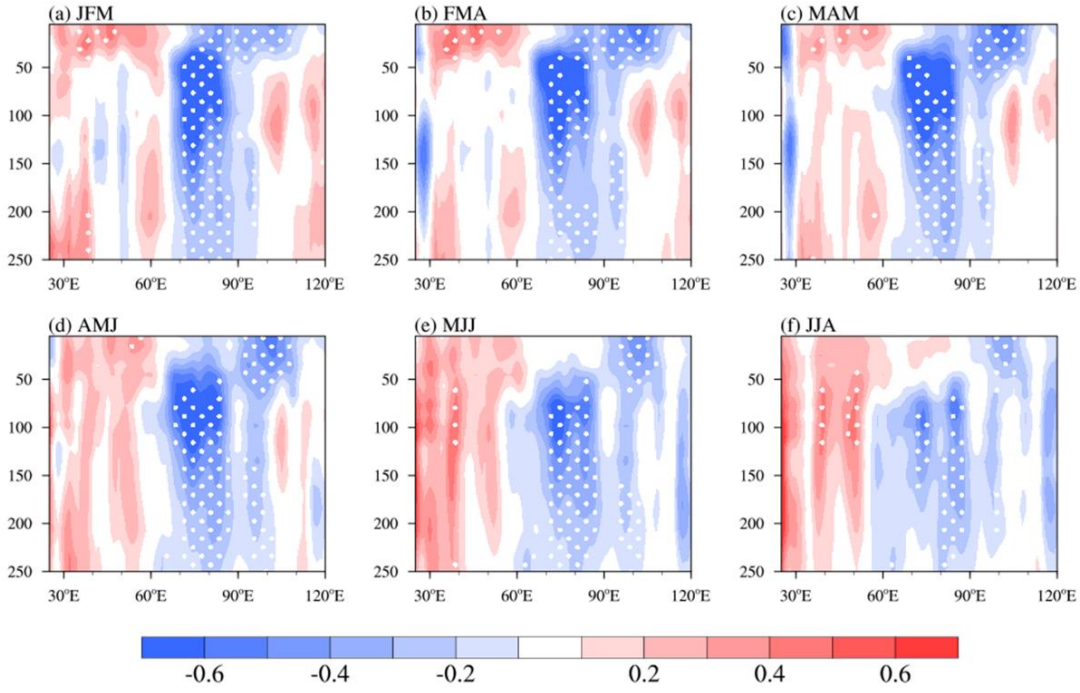

Figure S7. Composites of summer 5–45°S mean subsurface ocean temperature (unit: K) associated with the SIOD (i.e., SIODP minus SIODN) in (a) JFM, (b) FMA, (c) MAM, (d) AMJ, (e) MJJ, and (f) JJA from 1980 to 2019.The white dots indicate that the differences with shading was above the 90% confidence level.